Available online at http://scik.org
Commun. Math. Biol. Neurosci. 2026, 2026:65
https://doi.org/10.28919/cmbn/9953
ISSN: 2052-2541

MATHEMATICAL MODELLING OF TB–COVID-19 CO-INFECTION WITH TIME DELAY AND OPTIMAL CONTROL ANALYSIS

EDITH KATHURE KIUNYE[1,*], MARILYN RONOH[1], WESLEY NYALUKE[1],
JEREMIAH SAVALI KILONZI[2], EDNA CHILENJE MANDA[3]

[1]Department of Mathematics and Statistics, University of Embu, Embu, Kenya
[2]Department of Mathematics, Meru University of Science and Technology, Meru, Kenya
[3]Department of Mathematics, Mzuzu University, Luwinga, Malawi

Abstract. Tuberculosis (TB) and COVID–19 remains a major global public health threat, particularly in low- and middle-income countries where healthcare systems face persistent structural constraints. The co-existence of these two diseases introduces complex clinical and epidemiological challenges, such as delayed diagnosis, delayed treatment initiation and overlapping symptoms, which generally increase the disease burden and mortality risk. In this study, we formulate and analyse a deterministic compartmental model for TB–COVID–19 co-infection incorporating time delays representing diagnostic and treatment lags. The model integrates three public health interventions i.e. physical distancing, vaccination and treatment, formulated as time-dependent control functions. Qualitative analysis establishes positivity and boundedness of the solutions, existence of invariant regions and threshold dynamics governed by reproduction numbers. An optimal control framework is then introduced in our work to reduce the number of infections and also the implementation costs. Using Pontryagin's Maximum Principle, the corresponding Hamiltonian system and adjoint equations are derived, together with the necessary conditions for optimal controls. To further explore the impact of these interventions, numerical simulations are carried out using delay differential equation techniques combined with a forward–backward sweep method. The results suggests that applying multiple interventions simultaneously can significantly lower the prevalence of co-infection and related

*Corresponding author
E-mail address: miannat025@gmail.com
Received April 30, 2026

fatalities. However, the presence of delays reduces the overall effectiveness of these strategies.The model offers quantitative proof that effective management of TB and COVID-19 co-infection in nations with limited resources requires early diagnosis, quick treatment initiation, and coordinated intervention methods.

Keywords: COVID-19; Tuberculosis; TB–COVID-19 co-infection; mathematical modeling; optimal control; time delay; public health interventions.

2020 AMS Subject Classification: 92D30.

1. INTRODUCTION

The COVID-19 pandemic revealed serious weaknesses in international health systems, especially in areas where endemic infectious diseases like tuberculosis (TB) are already prevalent [1, 2]. While COVID-19 posed a significant strain on healthcare, infrastructure, diagnostics, and treatment capacity, tuberculosis continues to be one of the world's leading causes of infectious disease death [3, 4]. Due to overlapping respiratory symptoms, delayed diagnosis, and delayed access to healthcare facilities, the co-existence of COVID-19 and TB poses a compounded public health concern [5]. These difficulties have been made worse in low-resource environments, where health systems are frequently underfunded and delayed diagnosis and treatment initiation are common [6, 7].

Based on clinical and epidemiological data, those with co-existing diseases have much worse COVID-19 outcomes, and TB patients are more likely to have severe disease progression and mortality [5, 8]. Most symptoms overlap between COVID-19 and TB and can often result in delayed or incorrect diagnosis, which prolongs the disease transmission and worsens the illness to more severe stages [9]. Such delays represent critical epidemiological mechanisms that standard compartmental models often fail to capture, despite their central role in shaping real-world transmission dynamics [10, 11].

Mathematical modelling has proven to be a more powerful tool for understanding infectious disease dynamics and informing public health policy [12, 13]. However, most existing TB–COVID–19 co-infection models assume instantaneous transitions between disease states, thereby neglecting the realistic time delays associated with diagnosis, testing, treatment initiation, healthcare-seeking and intervention implementation [14, 15]. These assumptions limits

the capacity of these models to accurately represent real transmission processes and to evaluate the true effectiveness of control strategies.

This study addresses this gap by developing a TB–COVID–19 co-infection model that explicitly incorporates time delays alongside public health interventions. Three control strategies are considered i.e. physical distancing, vaccination and treatment. These interventions reflect realistic public health responses and enable the assessment of integrated disease management strategies [1, 2]. By incorporating time delays into the model structure, the framework allows systematic investigation of how diagnostic and treatment lags influence epidemic trajectories, disease burden and the overall effectiveness of control policies in co-endemic places.

2. Model Formulation

In order to explain the dynamics of COVID-19 and tuberculosis (TB) transmission in a human population, this work creates a deterministic compartmental model that takes into account the possibility of co-infection and re-infection. The birth rate is not expected to be equal to the death rate, and the total population at time t, represented by $N(t)$, is assumed to be a variable due to recruitment and disease-induced mortality. Nine epidemiological compartments are created based on the population's illness status i.e. susceptible to both infections $S(t)$, TB-exposed $E_b(t)$, active TB-infected but susceptible to COVID-19 $I_b(t)$, recovered from active TB infection $R_b(t)$, COVID-19 exposed $E_c(t)$, symptomatic COVID-19 infected but susceptible to TB $I_c(t)$, recovered from symptomatic COVID-19 infection $R_c(t)$, TB–COVID-19 co-infection $I_{b_c}(t)$ and recovered from TB–COVID-19 co-infection $R_{b_c}(t)$. Those who have not been exposed to either disease are the susceptible. Exposed individuals are in the latent stage of infection, infected individuals are those with active disease and capable of transmitting infection, while recovered individuals are those who have cleared infection through natural recovery or successful treatment, with immunity that may decrease over time.

Recruitment into the population occurs through a constant inflow into the susceptible class at rate λ. In addition, individuals who recover from TB, COVID-19 and co-infection may lose immunity and return to susceptibility. Specifically, transitions back to the susceptible class occur from the TB recovery class at rate θ_b, from the COVID-19 recovery class at rate θ_c, and from the co-infection recovery class at rate θ_{b_c}. All compartments are subject to natural

mortality at a constant per capita rate μ, while infected classes also experience disease-induced mortality.

COVID-19 transmission is governed by a nonlinear force of infection given by

$$\beta_c = \frac{\alpha\,(E_c + \eta I_c + \kappa I_{b_c})}{N},$$

where α is the COVID-19 transmission effective contact rate, η is the modification parameter of symptomatic COVID-19 individuals and κ accounts for the contribution of co-infected individuals to COVID-19 transmission. Susceptible individuals acquire COVID-19 infection and move into the exposed class E_c at rate $\rho_c\beta_c$. Individuals in the exposed class progress to the symptomatic infected class I_c at rate ω_c. Symptomatic COVID-19 individuals recover at rate γ_c, die due to disease at rate δ_c and are also subject to natural mortality at rate μ. Recovered COVID-19 individuals enter the class R_c, from which they may lose immunity and return to susceptibility at rate θ_c.

Similarly, TB transmission is described by the force of infection

$$\beta_b = \frac{\pi\,(E_b + \sigma I_b + \varphi I_{b_c})}{N},$$

where π is the TB transmission rate, σ modifies the infectiousness of individuals with active TB and φ represents the contribution of co-infected individuals to TB transmission. Susceptible individuals acquire TB infection and move into the TB-exposed class E_b at rate $\rho_b\beta_b$. Individuals in the TB-exposed class progress to active TB infection I_b at rate ω_b. Active TB-infected individuals recover at rate γ_b, die due to TB at rate δ_b, and are subject to natural mortality at rate μ. Individuals who recover from TB enter the class R_b, from which they may lose immunity and return to the susceptible class at rate θ_b.

Co-infection dynamics arise when individuals with active TB acquire COVID-19 infection or the vice versa. Thus, individuals in the active TB class I_b move into the co-infected class I_{b_c} at rate $\psi_c\beta_c$. Co-infected individuals may recover from both infections at rate γ_{b_c}, die due to co-infection at rate δ_{b_c} and are also subject to natural mortality at rate μ. Also, individuals in the active COVID-19 class I_c move into the co-infected class I_{b_c} at rate $\psi_c\beta_b$. Those who recover from co-infection enter the recovery class $R_{b_c}(t)$, from which they may lose immunity and return to susceptibility at rate θ_{b_c}.

The formulation of the model is based on the following assumptions: the population is homogeneously mixed; latent individuals are less infectious than symptomatic individuals; co-infected individuals contribute to the transmission of both TB and COVID-19; recovered individuals do not acquire permanent immunity and may return to susceptibility due to waning immunity; disease-induced mortality occurs only in infected classes; and all model parameters are non-negative constants. The total population size at time t is given by

$$N(t) = S + E_b + I_b + R_b + E_c + I_c + R_c + I_{b_c} + R.$$

For both qualitative and quantitative epidemiological analysis, this model formulation offers a biologically realistic and mathematically consistent framework for examining the transmission dynamics of COVID-19 and TB, including single infection, co-infection, recovery, re-infection, and disease-induced mortality.

TABLE 1. Model parameters, descriptions, and baseline values

Parameter	Description	Value	Source
λ	Recruitment rate	2143	Calculated
π	TB transmission rate	0.4	Estimated
α	COVID-19 transmission rate	0.5	Estimated
κ	Role of co-infected individuals to COVID-19 transmission	0.5	Estimated
φ	Role of co-infected individuals to TB transmission	0.6	Estimated
μ	Natural death rate	0.0143	Calculated
β_b	Force of infection for TB	0.3425 day^{-1}	[16]
ρ_b	Exposed rate to TB infection	0.6 day^{-1}	Estimated
ω_b	Exposed to TB to active TB progression	0.08 day^{-1}	Estimated
γ_b	TB recovery rate	0.2 day^{-1}	[17]
δ_b	TB-induced death rate	0.00032 day^{-1}	[18]
θ_b	Loss of TB immunity	0.0005 day^{-1}	[19]
β_c	Force of infection for COVID-19	0.476 day^{-1}	[20]
ρ_c	Exposed rate to COVID-19 infection	0.7 day^{-1}	Estimated
ω_c	Exposed to infectious (COVID-19)	0.05 day^{-1}	Estimated
γ_c	COVID-19 recovery rate	0.07 day^{-1}	Assumed
δ_c	COVID-19-induced death rate	0.02 day^{-1}	Assumed
θ_c	Loss of COVID-19 immunity	0.001	[19]
η	Infectious rate for COVID-19	0.9 day^{-1}	Fitted
σ	infectious rate for TB	0.6 day^{-1}	[21]
γ_{bc}	Recovery from co-infection	0.0055 day^{-1}	[17]
δ_{bc}	Co-infection induced death rate	0.03day^{-1}	[17]
θ_{bc}	Loss of immunity (co-infection)	0.001 day^{-1}	[Assumed]
ψ_b	TB infected individuals contract COVID-19	0.013 day^{-1}	[22]
ψ_c	COVID-19 infected individuals contract TB	0.0028 day^{-1}	[22]

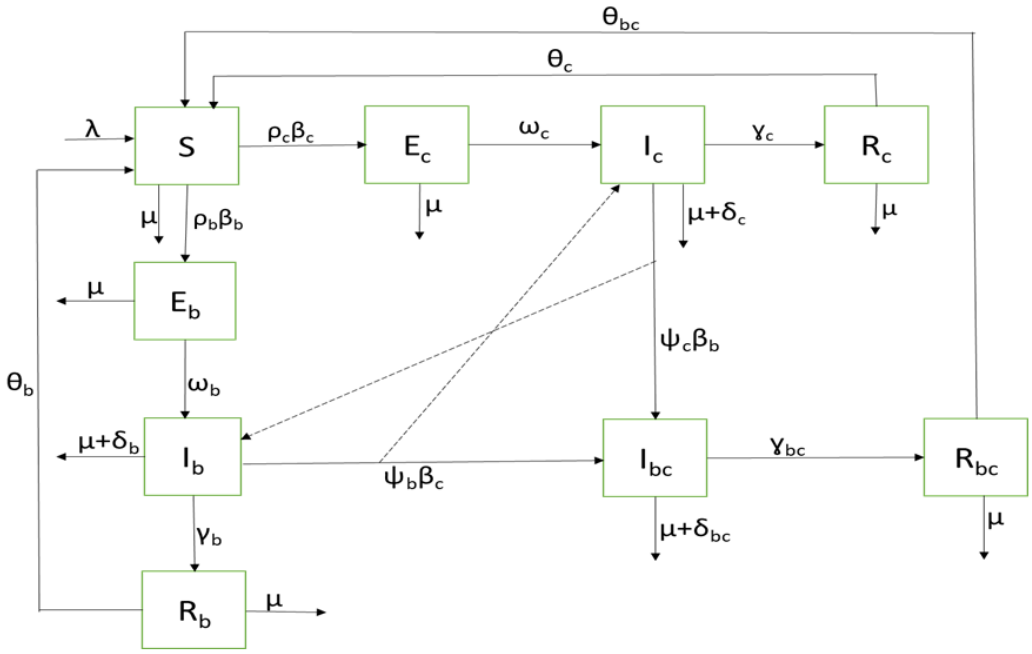

FIGURE 1. TB-COVID-19 compartmental model

2.1. Model equations.

$$\frac{dS}{dt} = \lambda + \theta_b R_b + \theta_c R_c + \theta_{b_c} R_{b_c} - (\mu + \rho_c\beta_c + \rho_b\beta_b)S \tag{1}$$

$$\frac{dE_c}{dt} = \rho_c\beta_c S - (\mu + \omega_c)E_c \tag{2}$$

$$\frac{dI_c}{dt} = \omega_c E_c - (\gamma_c + \mu + \delta_c + \psi_c\beta_b)I_c \tag{3}$$

$$\frac{dR_c}{dt} = \gamma_c I_c - (\mu + \theta_c)R_c \tag{4}$$

$$\frac{dE_b}{dt} = \rho_b\beta_b S - (\mu + \omega_b)E_b \tag{5}$$

$$\frac{dI_b}{dt} = \omega_b E_b - (\mu + \delta_b + \gamma_b)I_b \tag{6}$$

$$\frac{dR_b}{dt} = \gamma_b I_b(t - d_1) - (\mu + \theta_b)R_b \tag{7}$$

$$\frac{dI_{b_c}}{dt} = \psi_b\beta_c I_b + \psi_c\beta_b I_c - (\mu + \delta_{b_c} + \gamma_{b_c})I_{b_c}(t - d_2) \tag{8}$$

$$\frac{dR_{b_c}}{dt} = \gamma_{b_c} I_{b_c} - (\mu + \theta_{b_c})R_{b_c} \tag{9}$$

3. Model Analysis

3.1. Positivity.

Theorem 3.1. *Let* $R=(S,E_c,I_c,R_c,E_b,I_b,R_b,I_{b_c},R_{b_c})\in R_+^9:(S>0,E_c>0,I_c>0,R_c>0,E_b>0,I_b>0,R_b>0,I_{b_c}>0,R_{b_c}>0)$ *then the solutions of* $R=(S,E_c,I_c,R_c,E_b,I_b,R_b,I_{b_c},R_{b_c})$ *are all positive for all* $t\geq 0$ [23].

Proof. Let $S,E_c,I_c,R_c,E_b,I_b,R_b,I_{b_c}$ and R_{b_c} be a solution of the system with non-negative initial conditions. From the system of differential equations, we consider the equation (1),

$$\frac{dS}{dt}=\lambda+\theta_bR_b+\theta_cR_c+\theta_{b_c}R_{b_c}-(\mu+\rho_c\beta_c+\rho_b\beta_b)S \tag{10}$$

Since all parameters and state variables are non–negative, it follows that

$$\begin{aligned}
\frac{dS(t)}{dt}&\geq-(\mu+\rho_c\beta_c+\rho_b\beta_b)S(t),\\
\int\frac{dS(t)}{S(t)}&\geq-\int_0^t(\mu+\rho_c\beta_c+\rho_b\beta_b)dt,\\
\ln S(t)&\geq-\int_0^t(\mu+\rho_c\beta_c+\rho_b\beta_b)dt+c,\\
e^{\ln S(t)}&\geq e^{-\int_0^t(\mu+\rho_c\beta_c+\rho_b\beta_b)dt}e^c,\\
S(t)&\geq e^{-\int_0^t(\mu+\rho_c\beta_c+\rho_b\beta_b)dt}e^c. \qquad (11)
\end{aligned}$$

Applying the initial conditions to equation (11), that is, letting $t=0$, we have

$$S(0)\geq e^c,$$

therefore equation (11) becomes,

$$S(t)=S(0)e^{-\int_0^t(\mu+\rho_c\beta_c+\rho_b\beta_b)dt}\geq 0.$$

Similarly, if follows for equation (2) - (9) of the model, we follow comparable procedures to obtain;

$$\begin{aligned}
E_c(t)&=E_c(0)e^{-\int_0^t(\mu+\omega_c)\,dt}\geq 0,\\
I_c(t)&=I_c(0)e^{-\int_0^t(\mu+\delta_c+\psi_c\beta_b+\gamma_c)\,dt}\geq 0,\\
R_c(t)&=R_c(0)e^{-\int_0^t(\mu+\theta_c)\,dt}\geq 0,
\end{aligned}$$

$$E_b(t) = E_b(0)e^{-\int_0^t(\mu+\omega_b)\,dt} \geq 0,$$

$$I_b(t) = I_b(0)e^{-\int_0^t(\mu+\delta_b+\gamma_b)\,dt} \geq 0,$$

$$R_b(t) = R_b(0)e^{-\int_0^t(\mu+\theta_b)\,dt} \geq 0,$$

$$I_{b_c}(t) = I_{b_c}(0)e^{-\int_0^t(\mu+\delta_{b_c}+\gamma_{b_c}(t-d_2))\,dt} \geq 0,$$

$$R_{b_c}(t) = R_{b_c}(0)e^{-\int_0^t(\mu+\theta_{b_c})\,dt} \geq 0.$$

□

3.2. Invariant Region. Let the total human population be

$$N(t) = S + E_c + I_c + R_c + E_b + I_b + R_b + I_{b_c} + R_{b_c}.$$

Differentiating with respect to time t gives,

$$\frac{dN}{dt} = \frac{dS}{dt} + \frac{dE_c}{dt} + \frac{dI_c}{dt} + \frac{dR_c}{dt} + \frac{dE_b}{dt} + \frac{dI_b}{dt} + \frac{dR_b}{dt} + \frac{dI_{b_c}}{dt} + \frac{dR_{b_c}}{dt}.$$

Substituting the model equations and simplifying yields

$$\frac{dN}{dt} = \lambda - \mu N - \delta_b I_b - \delta_c I_c - \delta_{b_c} I_{b_c}. \tag{12}$$

In the absence of disease-induced deaths, that is $\delta_b = \delta_c = \delta_{b_c} = 0$, equation (12) reduces to

$$\frac{dN}{dt} \leq \lambda - \mu N. \tag{13}$$

Solving inequality (13) using the integrating factor method gives

$$N(t) \leq \frac{\lambda}{\mu}\left(1 - e^{-\mu t}\right) + N_0 e^{-\mu t}. \tag{14}$$

Hence, if $N_0 \leq \frac{\lambda}{\mu}$, then

$$N(t) \leq \frac{\lambda}{\mu}, \qquad \forall t \geq 0.$$

Therefore, the region

$$\Omega = \left\{ X \in \mathbb{R}_+^9 : N(t) \leq \frac{\lambda}{\mu} \right\}$$

is positively invariant and bounded, and all solutions remain biologically feasible.

3.3. Disease Free Equilibrium. To compute the DFE, we set the right hand side of the equations (1) - (9) to zero. On solving we obtained,

$$E_0 = (\frac{\lambda}{\mu}, 0, 0, 0, 0, 0, 0, 0, 0). \tag{15}$$

3.4. Basic reproduction number. The basic reproduction number R_0 was calculated using the next generation matrix. The classes E_c, I_c, E_b, I_b and I_{b_c} are implicated in the spread of COVID-19 and TB, according to equation (1)-(9). Consequently, the system of equations (1)-(9) can be expressed in simplified form as follows:

$$\begin{aligned}
\frac{dE_c}{dt} &= \rho_c \beta_c S - (\mu + \omega_c) E_c \\
\frac{dI_c}{dt} &= \omega_c E_c - (\gamma_c + \mu + \delta_c + \psi_c \beta_b) I_c \\
\frac{dE_b}{dt} &= \rho_b \beta_b S - (\mu + \omega_b) E_b \\
\frac{dI_b}{dt} &= \omega_b E_b - (\mu + \delta_b + \gamma_b) I_b \\
\frac{dI_{b_c}}{dt} &= \psi_b \beta_c I_b + \psi_c \beta_b I_c - (\mu + \delta_{b_c} + \gamma_{b_c}(t - d_2)) I_{b_c}
\end{aligned}$$

The transfer of infections inside the compartments is represented by $\mathscr{V}$, while the matrix $\mathscr{F}$ represents the new infections.

$$\mathscr{F} = \begin{pmatrix} \rho_c \beta_c S \\ 0 \\ \rho_b \beta_b S \\ 0 \\ \psi_b \beta_c I_b + \psi_c \beta_b I_c \end{pmatrix} \text{ and } \mathscr{V} = \begin{pmatrix} (\mu + \omega_c) E_c \\ -\omega_c E_c + (\gamma_c + \mu + \delta_c + \psi_c \pi (E_c + \sigma I_b + \varphi I_{b_c})) I_c \\ (\mu + \omega_b) E_b \\ -\omega_b E_b + (\mu + \delta_b + \gamma_b) I_b \\ (\mu + \delta_{b_c} + \gamma_{b_c}(t - d_2)) I_{b_c} \end{pmatrix} \tag{16}$$

The Jacobian of $\mathscr{F}$ and $\mathscr{V}$ with regard to E_c, I_c, E_b, I_b, and I_{b_c} evaluated at the disease-free equilibrium yields the transition matrices F and V as

$$F = \begin{pmatrix} \rho_c \alpha & \rho_c \alpha \eta & 0 & 0 & \rho_c \alpha \kappa \\ 0 & 0 & 0 & 0 & 0 \\ 0 & 0 & \rho_b \pi & \rho_b \pi \sigma & \rho_b \pi \varphi \\ 0 & 0 & 0 & 0 & 0 \\ 0 & 0 & 0 & 0 & 0 \end{pmatrix}, V = \begin{pmatrix} \mu + \omega_c & 0 & 0 & 0 & 0 \\ -\omega_c & \mu + \gamma_c + \delta_c & 0 & 0 & 0 \\ 0 & 0 & \mu + \omega_b & 0 & 0 \\ 0 & 0 & -\omega_b & \mu + \gamma_b + \delta_b & 0 \\ 0 & 0 & 0 & 0 & \mu + \delta_{b_c} + \gamma_{b_c} \end{pmatrix}.$$

The inverse of V is evaluated as,

$$V^{-1} = \begin{pmatrix} \frac{1}{\mu+\omega_c} & 0 & 0 & 0 & 0 \\ \frac{\omega_c}{(\mu+\omega_c)(\mu+\gamma_c+\delta_c)} & \frac{1}{\mu+\gamma_c+\delta_c} & 0 & 0 & 0 \\ 0 & 0 & \frac{1}{\mu+\omega_b} & 0 & 0 \\ 0 & 0 & \frac{\omega_b}{(\mu+\omega_b)(\mu+\gamma_b+\delta_b)} & \frac{1}{\mu+\gamma_b+\delta_b} & 0 \\ 0 & 0 & 0 & 0 & \frac{1}{\mu+\delta_{b_c}+\gamma_{b_c}} \end{pmatrix}$$

On computing $FV^{-}1$ we have,

$$FV^{-1} = \begin{pmatrix} \frac{\alpha\rho_c(\mu+\gamma_c+\delta_c+\eta\omega_c)}{(\mu+\gamma_c+\delta_c)(\mu+\omega_c)} & \frac{\alpha\eta\rho_c}{\mu+\gamma_c+\delta_c} & 0 & 0 & \frac{\alpha\kappa\rho_c}{\gamma_{b_c}+\mu+\delta_{b_c}} \\ 0 & 0 & 0 & 0 & 0 \\ 0 & 0 & \frac{\pi\rho_b(\mu+\gamma_b+\delta_b+\sigma\omega_b)}{(\mu+\gamma_b+\delta_b)(\mu+\omega_b)} & \frac{\pi\sigma\rho_b}{\gamma_b+\mu+\delta_b} & \frac{\pi\varphi\rho_b}{\gamma_{b_c}+\mu+\delta_{b_c}} \\ 0 & 0 & 0 & 0 & 0 \\ 0 & 0 & 0 & 0 & 0 \end{pmatrix}$$

The dominant eigenvalue represents the basic reproduction numbers, which are,

$$R_c = \frac{\rho_c\alpha(\mu+\gamma_c+\delta_c+\eta\,\omega_c)}{(\mu+\omega_c)(\mu+\gamma_c+\delta_c)}, \quad R_b = \frac{\rho_b\pi(\mu+\gamma_b+\delta_b+\sigma\,\omega_b)}{(\mu+\omega_b)(\mu+\gamma_b+\delta_b)}.$$

The basic reproduction number of the model is given by

$R_0 = \max\left\{R_c, R_b\right\}$

3.5. Local stability of Disease-Free Equilibrium (DFE). By block decomposition, the Jacobian matrix evaluated at the disease-free equilibrium can be partitioned into independent sub-blocks. Some eigenvalues are obtained directly from the diagonal structure of the decoupled compartments and are given by,

$$\lambda_1 = -\mu, \quad \lambda_2 = -(\mu+\theta_{b_c}), \quad \lambda_3 = -(\mu+\delta_{b_c}+\gamma_{b_c})(t-d_2), \quad \lambda_4 = -(\mu+\theta_b),$$

which are all strictly negative since all parameters represent positive biological rates. Hence, these modes are asymptotically stable.

The remaining dynamics are governed by the reduced Jacobian matrix

$$J(E_0^*) = \begin{pmatrix} \frac{\alpha\rho_c\lambda}{\mu} - (\mu+\omega_c) & \frac{\alpha\rho_c\eta\lambda}{\mu} & 0 & 0 & 0 \\ \omega_c & -(\gamma_c+\mu+\delta_c) & 0 & 0 & 0 \\ 0 & \gamma_c & -(\mu+\theta_c) & 0 & 0 \\ 0 & 0 & 0 & \frac{\rho_b\pi\lambda}{\mu} - (\mu+\omega_b) & \frac{\rho_b\pi\sigma\lambda}{\mu} \\ 0 & 0 & 0 & \omega_b & -(\mu+\delta_b+\gamma_b) \end{pmatrix}.$$

This matrix captures the transmission dynamics of the COVID-19 only and TB only subsystems and therefore determines the local stability of the disease-free equilibrium. The characteristic polynomial associated with this matrix is

$$\phi^5 + a_1\phi^4 + a_2\phi^3 + a_3\phi^2 + a_4\phi + a_5 = 0,$$

where the coefficients $a_i,\ i = 1,2,3,4,5$ are positive functions of the model parameters obtained using Mathematica software.

These coefficients are combinations of natural death rates, recovery rates, progression rates, and transmission terms. When the basic reproduction number satisfies $R_0 < 1$, the transmission terms are dominated by the removal, recovery, and mortality processes, which guarantees that

$$a_i > 0 \quad \text{for all } i = 1,2,3,4,5.$$

The Routh–Hurwitz criterion is used to ascertain the sign of the real parts of the characteristic polynomial's roots. The associated Routh table is constructed as follows:

$$\begin{array}{c|ccc} \phi^5 & 1 & a_2 & a_4 \\ \phi^4 & a_1 & a_3 & a_5 \\ \phi^3 & b_1 & b_2 & 0 \\ \phi^2 & c_1 & a_5 & 0 \\ \phi^1 & d_1 & 0 & 0 \\ \phi^0 & a_5 & 0 & 0 \end{array}$$

where

$$b_1 = \frac{a_1a_2 - a_3}{a_1}, \qquad b_2 = \frac{a_1a_4 - a_5}{a_1},$$

$$c_1 = \frac{b_1 a_3 - a_1 b_2}{b_1},$$

$$d_1 = \frac{c_1 b_2 - b_1 a_5}{c_1}.$$

The Routh–Hurwitz stability criterion states that if and only if every element in the first column of the Routh table is positive, then all roots of the characteristic polynomial have strictly negative real portions i.e.

$$1 > 0, \quad a_1 > 0, \quad b_1 > 0, \quad c_1 > 0, \quad d_1 > 0, \quad a_5 > 0.$$

When $R_0 < 1$, all transmission terms are subcritical and the removal and recovery terms dominate, implying

$$a_1 > 0,\ b_1 > 0,\ c_1 > 0,\ d_1 > 0,\ a_5 > 0,$$

and hence all Routh–Hurwitz conditions are satisfied. Therefore, all eigenvalues of the reduced Jacobian matrix have negative real parts, and the disease-free equilibrium E_0 is locally asymptotically stable.

Conversely, when $R_0 > 1$, at least one transmission term dominates the removal processes, causing violation of at least one Routh–Hurwitz positivity condition. This implies the existence of at least one eigenvalue with positive real part, and therefore the disease-free equilibrium E_0 becomes unstable.

Therefore, If $R_0 < 1$, the disease-free equilibrium is locally asymptotically stable and if $R_0 > 1$, it is unstable. This concludes the proof.

3.6. Global stability of the disease-free equilibrium. To investigate the global stability of the disease-free equilibrium (DFE), the Castillo–Chavez approach is employed. The model system is rewritten in the form,

$$\frac{dP}{dt} = F(P,Q), \qquad \frac{dQ}{dt} = G(P,Q), \qquad G(P,0) = 0,$$

where P denotes the uninfected population compartments and Q denotes the infected population compartments. Specifically,

$$P = (S, R_b, R_c, R_{b_c}), \qquad Q = (E_c, I_c, E_b, I_b, I_{b_c}).$$

The disease-free equilibrium is denoted by

$$U = (P^*, 0).$$

For the point $U = (P^*, 0)$ to be globally asymptotically stable, the following conditions must hold:

$$(\mathbf{H_1}): \quad \frac{dP}{dt} = F(P,0),\ P^* \text{ is globally asymptotically stable},$$

$$(\mathbf{H_2}): \quad G(P,Q) = KQ - \tilde{G}(P,Q), \quad \tilde{G}(P,Q) \geq 0 \text{ in } \Omega.$$

Theorem 3.2. *The disease-free equilibrium point $U = (P^*, 0)$ is globally asymptotically stable provided that $R_0 < 1$ and conditions (H_1) and (H_2) are satisfied.*

Proof. From the model equations, the functions $F(P,Q)$ and $G(P,Q)$ are obtained as

$$F(P,Q) = \begin{pmatrix} \lambda + \theta_b R_b + \theta_c R_c + \theta_{b_c} R_{b_c} - (\mu S + \rho_c \beta_c S + \rho_b \beta_b S) \\ \gamma_c I_c - (\mu + \theta_c) R_c \\ \gamma_b I_b(t - d_1) - (\mu + \theta_b) R_b \\ \gamma_{b_c} I_{b_c} - (\mu + \theta_{b_c}) R_{b_c} \end{pmatrix},$$

and hence

$$F(P,0) = \begin{pmatrix} \lambda - \mu S \\ 0 \\ 0 \\ 0 \end{pmatrix}.$$

The infected subsystem is given by

$$G(P,Q) = \begin{pmatrix} \rho_c \beta_c S - (\mu + \omega_c) E_c \\ \omega_c E_c - (\gamma_c + \mu + \delta_c + \psi_c \beta_b) I_c \\ \rho_b \beta_b S - (\mu + \omega_b) E_b \\ \omega_b E_b - (\mu + \delta_b + \gamma_b) I_b \\ \psi_b \beta_c I_b + \psi_c \beta_b I_c - (\mu + \delta_{b_c} + \gamma_{b_c}(t - d_2)) I_{b_c} \end{pmatrix}.$$

The Jacobian of $G(P,Q)$ with respect to Q evaluated at the disease-free equilibrium $U = (P^*, 0)$ is

$$K = D_Q G(U,0) = \begin{pmatrix} \rho_c\alpha - (\mu+\omega_c) & \rho_c\eta\alpha & 0 & 0 & \rho_c\alpha\kappa \\ \omega_c & -(\gamma_c+\mu+\delta_c) & 0 & 0 & 0 \\ 0 & 0 & \rho_b\pi - (\mu+\omega_b) & \rho_b\pi\sigma & \rho_b\pi\varphi \\ 0 & 0 & \omega_b & -(\mu+\delta_b+\gamma_b) & 0 \\ 0 & 0 & 0 & 0 & -(\mu+\delta_{b_c}+\gamma_{b_c}(t-d_2)) \end{pmatrix}$$

Where K is a Metzler matrix.

Lets define

$$\tilde{G}(P,Q) = KQ - G(P,Q).$$

Then

$$\tilde{G}(P,Q) = \begin{pmatrix} \rho_c\alpha E_c + \rho_c\eta\alpha I_c + \rho_c\alpha I_{b_c} - \rho_c\beta_c S \\ 0 \\ \rho_b\pi E_b + \rho_b\pi\sigma I_b + \rho_b\pi I_{b_c} - \rho_b\beta_b S \\ 0 \\ \psi_b\beta_c I_b + \psi_c\beta_b I_c \end{pmatrix}.$$

$$KQ - G(P,Q) = \begin{pmatrix} \rho_c\alpha E_c + \rho_c\eta\alpha I_c + \rho_c\alpha\kappa I_{b_c} - \rho_c\beta_c S \\ \psi_c\beta_b I_c \\ \rho_b\pi E_b + \rho_b\pi\sigma I_b + \rho_b\pi\varphi I_{b_c} - \rho_b\beta_b S \\ 0 \\ -\psi_b\beta_c I_b - \psi_c\beta_b I_c \end{pmatrix}$$

Since $S/N \leq 1$ in the feasible region Ω and all parameters are non-negative biological rates, it follows that

$$\tilde{G}(P,Q) \geq 0 \quad \text{for all } (P,Q) \in \Omega.$$

Thus, condition (H_2) is satisfied.

For condition (H_1), the reduced uninfected subsystem

$$\frac{dP}{dt} = F(P,0)$$

has a globally asymptotically stable equilibrium P^*, since it is linear, decoupled, and governed by negative definite dynamics with a unique equilibrium solution.

Therefore, both conditions (H_1) and (H_2) of the Castillo–Chavez theorem are satisfied. Hence, the disease-free equilibrium $U = (P^*, 0)$ is globally asymptotically stable whenever

$$R_0 < 1.$$

This concludes the proof. □

3.7. The existence of endemic equilibrium point. The endemic equilibrium point, denoted by

$$E^*_{t_c} = (S^*, E^*_c, I^*_c, R^*_c, E^*_b, I^*_b, R^*_b, I^*_{b_c}, R^*_{b_c}),$$

corresponds to the persistent presence of the diseases in the community. To obtain the endemic equilibrium, all time derivatives in the model system are set equal to zero and the resulting algebraic system is solved simultaneously.

This yields the following equilibrium relations:

(17)
$$\begin{cases}
S^* = \dfrac{\theta_b R^*_b + \theta_{bc} R^*_{bc} + \theta_c R^*_c + \lambda}{\beta_b \rho_b + \beta_c \rho_c + \mu}, \\
E^*_c = \dfrac{\beta_c \rho_c \left(\theta_b R^*_b + \theta_{bc} R^*_{bc} + \theta_c R^*_c + \lambda\right)}{(\omega_c + \mu)(\beta_b \rho_b + \beta_c \rho_c + \mu)}, \\
R^*_c = \dfrac{\gamma_c I^*_c}{\theta_c + \mu}, \\
E^*_b = \dfrac{\beta_b \rho_b \left[(\theta_c + \mu)(\theta_b R^*_b + \theta_{bc} R^*_{bc} + \lambda) + \theta_c \gamma_c I^*_c\right]}{(\omega_b + \mu)(\theta_c + \mu)(\beta_b \rho_b + \beta_c \rho_c + \mu)}, \\
R^*_b = \dfrac{\gamma_b I^*_b(t - d_1)}{\theta_b + \mu}, \\
R^*_{bc} = \dfrac{\gamma_{bc} I^*_{bc}}{\theta_{bc} + \mu}, \\
I^*_c = \dfrac{\beta_c \rho_c \omega_c (\theta_b + \mu)(\theta_{bc} + \mu)\left[\lambda\mu + \theta_{bc}(\lambda + \gamma_{bc} I^*_{bc})\right]}{(\theta_b + \mu)(\theta_{bc} + \mu)(\omega_c + \mu)(\beta_b \rho_b + \beta_c \rho_c + \mu)\mathscr{D}_c}, \\
I^*_b = \dfrac{\beta_b \rho_b \omega_b (\theta_c + \mu)(\omega_c + \mu)\left[\lambda\mu + \theta_{bc}(\lambda + \gamma_{bc} I^*_{bc})\right](\beta_b \psi_c + \gamma_c + \delta_c + \mu)}{(\omega_b + \mu)(\theta_{bc} + \mu)\mathscr{D}_b}, \\
I^*_{bc} = \dfrac{\lambda\, \beta_b \beta_c \rho_c \psi_c \omega_c (\mu^2 + \mu\theta_b + \mu\theta_{bc} + \theta_b \theta_{bc})}{D} \Bigg/ \left[\dfrac{\beta_b \beta_c \gamma_{bc} \rho_c \psi_c \omega_c (\mu + \theta_b)\theta_{bc}}{D} - \mu - \gamma_{bc}(t - d_2) - \delta_{bc}\right].
\end{cases}$$

where the auxiliary expressions are defined as

$$\mathscr{D}_c = \gamma_c\Big[\omega_c\big((\theta_c+\mu)(\beta_b\rho_b+\mu)+\mu\beta_c\rho_c\big)+\mu(\theta_c+\mu)(\beta_b\rho_b+\beta_c\rho_c+\mu)\Big]$$
$$+(\theta_c+\mu)(\omega_c+\mu)(\beta_b\rho_b+\beta_c\rho_c+\mu)(\beta_b\psi_c+\delta_c+\mu),$$
$$\mathscr{D}_b = \gamma_b\left(1-\frac{\beta_b\theta_b\rho_b\omega_b(t-d_1)(\theta_c+\mu)(\omega_c+\mu)(\beta_b\psi_c+\gamma_c+\delta_c+\mu)}{(\theta_b+\mu)(\omega_b+\mu)\,\mathscr{D}_c}\right)+\delta_b+\mu,$$
$$D_1 = (\mu+\theta_b)(\mu+\theta_{bc})(\mu+\beta_b\rho_b+\beta_c\rho_c)(\mu+\omega_c),$$
$$D_2 = \mu+\delta_c+\beta_b\psi_c+\gamma_c\left(1-\frac{\beta_c\theta_c\rho_c\omega_c}{(\mu+\theta_c)(\mu+\beta_b\rho_b+\beta_c\rho_c)(\mu+\omega_c)}\right),$$
$$D = D_1D_2.$$

When all components of $E^*_{t_c}$ are positive, the endemic equilibrium point exists and is biologically feasible. This occurs when the basic reproduction number $R_0 > 1$. The presence of an endemic equilibrium point indicates that the diseases continue to persist in the population, with all infected compartments remaining active over time.

3.8. Global stability of the endemic equilibrium point. To investigate the global asymptotic stability of the endemic equilibrium point of the model, we apply LaSalle's Invariance Principle.

Theorem 3.3. *The endemic equilibrium point $E^*_{t_c}$ of the system is globally asymptotically stable in the feasible region Ω whenever $R_0 > 1$.*

Proof. Let

$$E^*_{t_c} = (S^*, E^*_c, I^*_c, R^*_c, E^*_b, I^*_b, R^*_b, I^*_{b_c}, R^*_{b_c})$$

denote the endemic equilibrium point of the model, where all components are strictly positive when $R_0 > 1$. The feasible region $\Omega \subset \mathbb{R}^9_+$ represents the biologically meaningful region in which all solutions of the system remain non–negative and bounded for all $t \geq 0$.

We define the Lyapunov function

$$\begin{aligned} L = {} & (S-S^*-S^*\ln\tfrac{S}{S^*})+(E_c-E^*_c-E^*_c\ln\tfrac{E_c}{E^*_c})+(I_c-I^*_c-I^*_c\ln\tfrac{I_c}{I^*_c}) \\ & +(R_c-R^*_c-R^*_c\ln\tfrac{R_c}{R^*_c})+(E_b-E^*_b-E^*_b\ln\tfrac{E_b}{E^*_b})+(I_b-I^*_b-I^*_b\ln\tfrac{I_b}{I^*_b}) \\ & +(R_b-R^*_b-R^*_b\ln\tfrac{R_b}{R^*_b})+(I_{b_c}-I^*_{b_c}-I^*_{b_c}\ln\tfrac{I_{b_c}}{I^*_{b_c}})+(R_{b_c}-R^*_{b_c}-R^*_{b_c}\ln\tfrac{R_{b_c}}{R^*_{b_c}}). \end{aligned} \tag{18}$$

For each state variable x, the function $x - x^* - x^* \ln \frac{x}{x^*}$ is non–negative for all $x > 0$ and vanishes only at $x = x^*$. Hence, $L \geq 0$ in Ω, and $L = 0$ if and only if

$$(S, E_c, I_c, R_c, E_b, I_b, R_b, I_{b_c}, R_{b_c}) = E^*_{t_c}.$$

Therefore, L is positive definite with respect to the endemic equilibrium point $E^*_{t_c}$.

Differentiating L with respect to time along solutions of the system gives;

$$\begin{aligned}\frac{dL}{dt} &= \left(1 - \frac{S^*}{S}\right)\frac{dS}{dt} + a_1\left(1 - \frac{E^*_c}{E_c}\right)\frac{dE_c}{dt} + a_2\left(1 - \frac{I^*_c}{I_c}\right)\frac{dI_c}{dt} + a_3\left(1 - \frac{R^*_c}{R_c}\right)\frac{dR_c}{dt} \\ &\quad + a_4\left(1 - \frac{E^*_b}{E_b}\right)\frac{dE_b}{dt} + a_5\left(1 - \frac{I^*_b}{I_b}\right)\frac{dI_b}{dt} + a_6\left(1 - \frac{R^*_b}{R_b}\right)\frac{dR_b}{dt} \\ &\quad + a_7\left(1 - \frac{I^*_{b_c}}{I_{b_c}}\right)\frac{dI_{b_c}}{dt} + a_8\left(1 - \frac{R^*_{b_c}}{R_{b_c}}\right)\frac{dR_{b_c}}{dt} \qquad (19)\end{aligned}$$

Substituting the right–hand side of the model equations into $\dot{L}$, and using the equilibrium relations satisfied by $E^*_{t_c}$, the resulting expression for $\dot{L}$ can be rearranged into a sum of non–positive terms using standard inequalities we obtain,

$$\dot{L} \leq 0 \quad \text{for all } (S, \ldots, R_{b_c}) \in \Omega.$$

Moreover, equality $\dot{L} = 0$ holds if and only if each term in the Lyapunov function vanishes, which occurs precisely when

$$S = S^*,\ E_c = E^*_c,\ I_c = I^*_c,\ R_c = R^*_c,\ E_b = E^*_b,\ I_b = I^*_b,\ R_b = R^*_b,\ I_{b_c} = I^*_{b_c},\ R_{b_c} = R^*_{b_c}.$$

Hence, the largest invariant set contained in

$$\{(S, E_c, I_c, R_c, E_b, I_b, R_b, I_{b_c}, R_{b_c}, R_{b_c}) \in \Omega : \dot{L} = 0\}$$

is the singleton set $\{E^*_{t_c}\}$.

By LaSalle's Invariance Principle, every solution of the system that starts in the feasible region Ω converges to $E^*_{t_c}$ as $t \to \infty$. Consequently, whenever $R_0 > 1$, the endemic equilibrium point $E^*_{t_c}$ is globally asymptotically stable in Ω. □

3.9. Bifurcation analysis. To analyze changes in the qualitative behavior of equilibria, the Center Manifold Theory developed by Castillo–Chavez and Song is employed. We introduce the change of variables

$$S = x_1,\ E_c = x_2,\ I_c = x_3,\ R_c = x_4,\ E_b = x_5,\ I_b = x_6,\ R_b = x_7,\ I_{b_c} = x_8,\ R_{b_c} = x_9,$$

and define the state vector

$$X = (x_1, x_2, x_3, x_4, x_5, x_6, x_7, x_8, x_9)^T.$$

Hence, the model can be written compactly as

$$\frac{dX}{dt} = F(X), \qquad F = (f_1, f_2, f_3, f_4, f_5, f_6, f_7, f_8, f_9)^T,$$

with

$$\begin{cases} \dot{x}_1 = \lambda + \theta_b x_7 + \theta_c x_4 + \theta_{b_c} x_9 - (\mu + \rho_c \beta_c + \rho_b \beta_b) x_1, \\ \dot{x}_2 = \rho_c \beta_c x_1 - (\mu + \omega_c) x_2, \\ \dot{x}_3 = \omega_c x_2 - (\gamma_c + \mu + \delta_c + \psi_c \beta_b) x_3, \\ \dot{x}_4 = \gamma_c x_3 - (\mu + \theta_c) x_4, \\ \dot{x}_5 = \rho_b \beta_b x_1 - (\mu + \omega_b) x_5, \\ \dot{x}_6 = \omega_b x_5 - (\mu + \delta_b + \gamma_b) x_6, \\ \dot{x}_7 = \gamma_b x_6(t - d_1) - (\mu + \theta_b) x_7, \\ \dot{x}_8 = \psi_b \beta_c x_6 + \psi_c \beta_b x_3 - (\mu + \delta_{b_c} + \gamma_{b_c}(t - d_2)) x_8, \\ \dot{x}_9 = \gamma_{b_c} x_8 - (\mu + \theta_{b_c}) x_9, \end{cases} \tag{20}$$

where

$$\beta_b = \frac{\pi(x_5 + \sigma x_6 + \kappa x_8)}{N}, \qquad \beta_c = \frac{\alpha(x_2 + \eta x_3 + \varphi x_8)}{N}.$$

Let E_0 denote the disease-free equilibrium. The Jacobian matrix evaluated at DFE is denoted by $J(E_0)$. At $R_0^b = 1$, the Jacobian has a simple zero eigenvalue, while all other eigenvalues have negative real parts, satisfying the hypotheses of the Castillo–Chavez–Song theorem.

Let $b = (b_1, b_2, b_3, b_4, b_5, b_6, b_7, b_9)^T$ be the right eigenvector of $J(E_0)$ associated with the zero eigenvalue, and $d = (d_1, d_2, d_3, d_4, d_5, d_6, d_7, d_8, d_9)^T$ the corresponding left eigenvector, normalized such that

$$d \cdot b = 1.$$

Let π be the bifurcation parameter and define $\pi = \pi^*$ such that $R_0^b = 1$. Solving $R_0^b = 1$ yields

$$\pi^* = \frac{(\mu + \gamma_b + \delta_b)(\mu + \omega_b)}{\rho_b(\mu + \gamma_b + \delta_b + \sigma\omega_b)}.$$

Consider the general system

$$\dot{X} = F(X, \pi), \qquad F \in C^2(\mathbb{R}^9 \times \mathbb{R}),$$

with equilibrium at $X = 0$ when $\pi = \pi^*$. Define the coefficients

$$a = \sum_{k,i,j=1}^{9} d_k b_i b_j \frac{\partial^2 f_k}{\partial x_i \partial x_j}(0, \pi^*), \qquad b = \sum_{k,i=1}^{9} d_k b_i \frac{\partial^2 f_k}{\partial x_i \partial \pi}(0, \pi^*).$$

According to the Center Manifold Theorem, the local dynamics near $(0, \pi^*)$ are completely determined by the signs of a and b:

i. $a > 0$, $b > 0$: backward (subcritical) bifurcation;

ii. $a < 0$, $b < 0$: forward (supercritical) bifurcation;

iii. $a > 0$, $b < 0$: saddle-node structure;

iv. $a < 0$, $b > 0$: transcritical forward bifurcation.

Computing the second-order partial derivatives and substituting into the expressions for a and b we obtain,

$$a > 0, \qquad b > 0.$$

Therefore, the model undergoes a backward bifurcation at $R_0^b = 1$, implying that a stable endemic equilibrium coexists with a stable disease-free equilibrium when $R_0^b < 1$. Hence, disease persistence is possible even when the basic reproduction number is less than unity.

This shows the presence of backward bifurcation in the model at $R_0^b = 1$.

3.10. Optimal Control Analysis. To assess the impact of intervention strategies on the transmission dynamics of the TB–COVID-19 co-infection model, optimal control theory is employed. Three time–dependent control functions are introduced i.e. $u_1(t)$, representing public health distancing measures aimed at reducing effective contact rates, $u_2(t)$, representing vaccination of susceptible individuals which moves individuals out of the susceptible class or reduces susceptibility and $u_3(t)$, representing treatment of infected individuals aimed at increasing recovery rates and reducing disease–induced mortality.

The acceptable control set is defined as follows, assuming that the controls are bounded and Lebesgue measurable.

$$\mathscr{U} = \{(u_1, u_2, u_3) : 0 \leq u_i(t) \leq 1,\ i = 1,2,3,\ \forall t \in [0,T]\}. \tag{21}$$

The controlled TB–COVID-19 co-infection model is given by

$$\begin{cases} \dfrac{dS}{dt} = \lambda + \theta_b R_b + \theta_c R_c + \theta_{b_c} R_{b_c} - (1-u_1(t))(\rho_c\beta_c + \rho_b\beta_b)S - (\mu + u_2(t))S, \\ \dfrac{dE_c}{dt} = (1-u_1(t))\rho_c\beta_c S - (\mu+\omega_c)E_c, \\ \dfrac{dI_c}{dt} = \omega_c E_c - (\mu + \delta_c + \psi_c\beta_b + \gamma_c + u_3(t))I_c, \\ \dfrac{dR_c}{dt} = (\gamma_c + u_3(t))I_c - (\mu+\theta_c)R_c, \\ \dfrac{dE_b}{dt} = (1-u_1(t))\rho_b\beta_b S - (\mu+\omega_b)E_b, \\ \dfrac{dI_b}{dt} = \omega_b E_b - (\mu + \delta_b + \gamma_b + u_3(t))I_b, \\ \dfrac{dR_b}{dt} = (\gamma_b + u_3(t))I_b(t-d_1) - (\mu+\theta_b)R_b, \\ \dfrac{dI_{b_c}}{dt} = (1-u_1(t))\big(\psi_b\beta_c I_b + \psi_c\beta_b I_c\big) - (\mu + \delta_{b_c} + \gamma_{b_c}(t-d_2) + u_3(t))I_{b_c}, \\ \dfrac{dR_{b_c}}{dt} = (\gamma_{b_c} + u_3(t))I_{b_c} - (\mu+\theta_{b_c})R_{b_c}. \end{cases} \tag{22}$$

The objective is to minimize the burden of COVID-19 infection, TB infection, and TB–COVID-19 co-infection, together with the costs associated with implementing the control strategies. The objective functional is defined by

$$\begin{aligned} J(u_1,u_2,u_3) = \int_0^T \Big[& A_1 I_c(t) + A_2 I_b(t) + A_3 I_{b_c}(t) \\ & + \tfrac{1}{2}\big(B_1 u_1^2(t) + B_2 u_2^2(t) + B_3 u_3^2(t)\big)\Big]\,dt, \end{aligned} \tag{23}$$

where $A_i > 0$ are weight parameters associated with the infected populations and $B_i > 0$ represent the relative costs of implementing the control strategies.

Let

$$\xi = (\xi_S, \xi_{E_c}, \xi_{I_c}, \xi_{R_c}, \xi_{E_b}, \xi_{I_b}, \xi_{R_b}, \xi_{I_{b_c}}, \xi_{R_{b_c}})$$

denote the adjoint variables corresponding to the state variables. The Hamiltonian $\mathscr{H}$ is defined by

$$\mathscr{H} = L + \sum_i \xi_i f_i,$$

where L is the integrand of the objective functional and f_i denote the right–hand sides of the controlled system. Explicitly

$$\begin{aligned}
\mathscr{H} &= A_1 I_c + A_2 I_b + A_3 I_{b_c} + \tfrac{1}{2}(B_1 u_1^2 + B_2 u_2^2 + B_3 u_3^2) \\
&+ \xi_S \Big[\lambda + \theta_b R_b + \theta_c R_c + \theta_{b_c} R_{b_c} - (1-u_1)(\rho_c \beta_c + \rho_b \beta_b) S - (\mu + u_2) S\Big] \\
&+ \xi_{E_c} \Big[(1-u_1)\rho_c \beta_c S - (\mu + \omega_c) E_c\Big] \\
&+ \xi_{I_c} \Big[\omega_c E_c - (\mu + \delta_c + \psi_c \beta_b + \gamma_c + u_3) I_c\Big] \\
&+ \xi_{R_c} \Big[(\gamma_c + u_3) I_c - (\mu + \theta_c) R_c\Big] \\
&+ \xi_{E_b} \Big[(1-u_1)\rho_b \beta_b S - (\mu + \omega_b) E_b\Big] \\
&+ \xi_{I_b} \Big[\omega_b E_b - (\mu + \delta_b + \gamma_b + u_3) I_b\Big] \\
&+ \xi_{R_b} \Big[(\gamma_b + u_3) I_b(t-d_1) - (\mu + \theta_b) R_b\Big] \\
&+ \xi_{I_{b_c}} \Big[(1-u_1)(\psi_b \beta_c I_b + \psi_c \beta_b I_c) - (\mu + \delta_{b_c} + \gamma_{b_c}(t-d_2) + u_3) I_{b_c}\Big] \\
&+ \xi_{R_{b_c}} \Big[(\gamma_{b_c} + u_3) I_{b_c} - (\mu + \theta_{b_c}) R_{b_c}\Big].
\end{aligned}$$

By Pontryagin's Maximum Principle, the adjoint variables satisfy

$$\frac{d\xi_i}{dt} = -\frac{\partial \mathscr{H}}{\partial x_i}, \qquad \xi_i(T) = 0, \tag{24}$$

where x_i denote the state variables. The adjoint equations associated with the infected compartments are given by

$$\begin{aligned}
\frac{d\xi_{I_c}}{dt} &= -A_1 + \xi_{I_c}(\mu + \delta_c + \psi_c \beta_b + \gamma_c + u_3) - \xi_{R_c}(\gamma_c + u_3) - \xi_{I_{b_c}}(1-u_1)\psi_c \beta_b, \\
\frac{d\xi_{I_b}}{dt} &= -A_2 + \xi_{I_b}(\mu + \delta_b + \gamma_b + u_3) - \xi_{R_b}(\gamma_b + u_3) - \xi_{I_{b_c}}(1-u_1)\psi_b \beta_c, \\
\frac{d\xi_{I_{b_c}}}{dt} &= -A_3 + \xi_{I_{b_c}}(\mu + \delta_{b_c} + \gamma_{b_c}(t-d_2) + u_3) - \xi_{R_{b_c}}(\gamma_{b_c} + u_3).
\end{aligned}$$

The optimal controls are obtained by minimizing the Hamiltonian pointwise with respect to u_1, u_2, and u_3 over the admissible set $\mathscr{U}$. Hence, the characterizations of the optimal controls

are given by

$$u_1^*(t) = \min\left\{1, \max\left(0, \frac{(\xi_{E_c} - \xi_S)\rho_c\beta_c S + (\xi_{E_b} - \xi_S)\rho_b\beta_b S + \xi_{I_{b_c}}(\psi_b\beta_c I_b + \psi_c\beta_b I_c)}{B_1}\right)\right\},$$

$$u_2^*(t) = \min\left\{1, \max\left(0, \frac{\xi_S S}{B_2}\right)\right\},$$

$$u_3^*(t) = \min\left\{1, \max\left(0, \frac{(\xi_{I_c} - \xi_{R_c})I_c + (\xi_{I_b} - \xi_{R_b})I_b + (\xi_{I_{b_c}} - \xi_{R_{b_c}})I_{b_c}}{B_3}\right)\right\}.$$

The existence of an optimal control triple (u_1^*, u_2^*, u_3^*) along with the corresponding optimal state and adjoint variables follows from standard results in optimal control theory because the control set $\mathscr{U}$ is nonempty, closed, and convex, the state system is bounded and Lipschitz continuous in the state variables, and the integrand of the objective functional is convex in the controls.

3.11. Uniqueness of the optimality system.

Theorem 3.4. *The optimality system associated with the delayed TB–COVID–19 optimal control problem admits a unique solution on the interval* $[0, T]$.

Proof. Let (X_1, Λ_1, U_1) and (X_2, Λ_2, U_2) be two solutions of the optimality system with the same initial conditions for the state variables and the same terminal conditions for the adjoint variables. Let

$$\Delta X = X_1 - X_2, \qquad \Delta\Lambda = \Lambda_1 - \Lambda_2, \qquad \Delta U = U_1 - U_2.$$

By the smoothness of the state and adjoint dynamics, the right-hand side of the state and adjoint systems are Lipschitz continuous with respect to their arguments. Hence, there exist constants $L_1, L_2 > 0$ such that

$$\|\Delta X'(t)\| \le L_1\big(\|\Delta X(t)\| + \|\Delta X(t-\tau)\| + \|\Delta U(t)\|\big),$$

$$\|\Delta\Lambda'(t)\| \le L_2\big(\|\Delta X(t)\| + \|\Delta X(t-\tau)\| + \|\Delta\Lambda(t)\| + \|\Delta\Lambda(t+\tau)\| + \|\Delta U(t)\|\big).$$

Moreover, the optimal control characterizations are given by projection operators onto closed convex sets. Since projection mappings are Lipschitz continuous, there exists $L_3 > 0$ such that

$$\|\Delta U(t)\| \le L_3\big(\|\Delta X(t)\| + \|\Delta X(t-\tau)\| + \|\Delta\Lambda(t)\|\big).$$

Let

$$\Phi(t) = \|\Delta X(t)\|^2 + \|\Delta\Lambda(t)\|^2.$$

Using the above estimates and Young's inequality, we obtain,

$$\frac{d}{dt}\Phi(t) \leq C\big(\Phi(t) + \Phi(t-\tau) + \Phi(t+\tau)\big),$$

for some constant $C > 0$.

Using the initial and terminal conditions

$$\Delta X(0) = 0, \qquad \Delta\Lambda(T) = 0,$$

and standard arguments for delay differential inequalities, it follows that

$$\Phi(t) \leq C\int_0^t \Phi(s)\,ds.$$

By Gronwall's inequality, $\Phi(t) = 0$ for all $t \in [0,T]$. Hence,

$$\Delta X(t) = 0, \qquad \Delta\Lambda(t) = 0, \qquad \Delta U(t) = 0 \quad \forall t \in [0,T].$$

Therefore, the optimal system admits a unique solution on $[0,T]$. □

3.12. Numerical simulation. The numerical simulations were performed to investigate the transmission dynamics of the TB–COVID–19 coinfection model and to evaluate the effectiveness of the proposed optimal control strategies. The simulation results are presented in Figures 2–6.

Figure 2 illustrates the epidemiological dynamics of the model compartments over time. In Figure 2a, the trajectories of the infected populations for COVID–19 (I_c), tuberculosis (I_b), and the co-infected class (I_{bc}) are presented.The findings indicate that active disease transmission among the susceptible population initially led to an increase in the number of affected persons. However, the infections progressively decline as the best control tactics are put into practice, suggesting that the intervention measures successfully lower the disease transmission.

The exposed populations for both diseases are shown in Figure 2b. When susceptible people come into contact with infectious people, the exposed classes first rise. The exposed populations decline as the control methods start to work, indicating that fewer people are reaching the

infectious stage. This illustrates how crucial preventive measures are to lowering the number of new illnesses.

The recovery dynamics are illustrated in Figure 2c. As infected individuals receive treatment and recover from their illnesses, the recovered populations gradually grow over time. The rise in people who have recovered shows how well treatment interventions work to shorten the period of infection and enhance recovery rates.

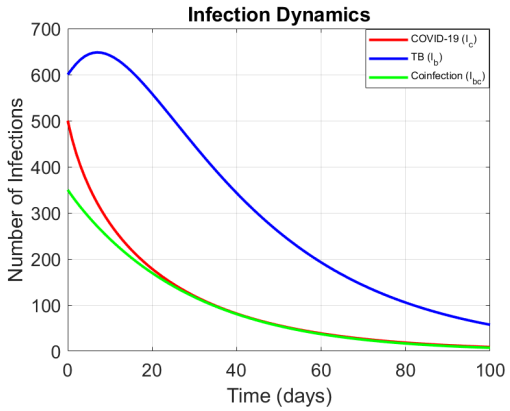

(A) Infection dynamics

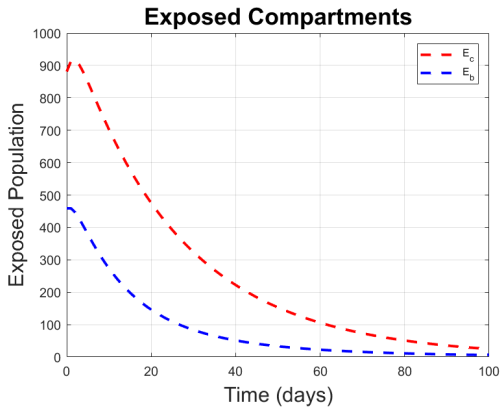

(B) Exposed compartments

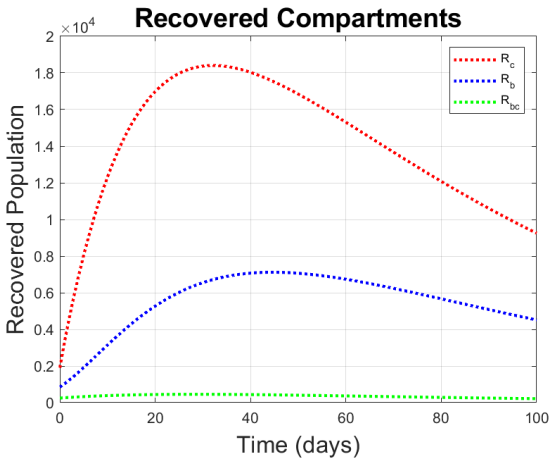

(C) Recovered compartments

FIGURE 2. Dynamics of TB and COVID-19 compartments over time.

The impact of the intervention strategies is further illustrated in Figure 3. The optimal control profiles shown in Figure 3a shows how the intervention strategies intensity varies during the simulation. Early in the epidemic, when infection levels are high, higher control levels are implemented; as the number of infections drops, the control intensity progressively reduces.

Figure 3b shows the dynamics of the susceptible and vaccinated populations. As vaccination is implemented, the number of vaccinated individuals increases while the susceptible population decreases, indicating the effectiveness of vaccination in protecting individuals from infection.

The reduction in the peak number of infected individuals is illustrated in Figure 3c. The results show that the introduction of optimal control strategies significantly lowers the maximum number of infections during the epidemic, thereby reducing the overall disease burden.

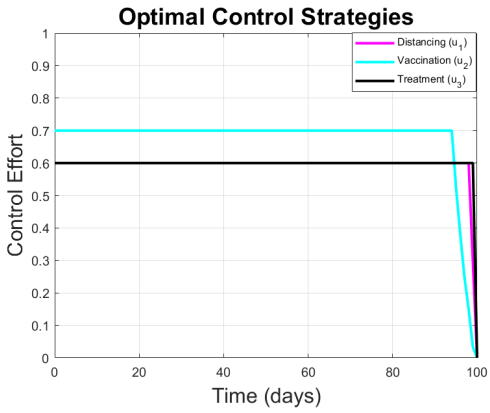

(A) Optimal control profiles

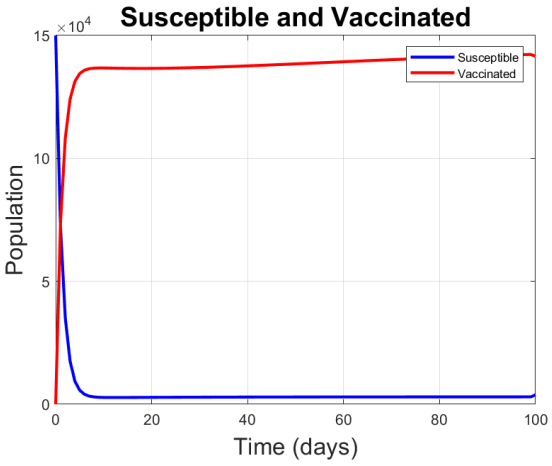

(B) Susceptible and vaccinated population

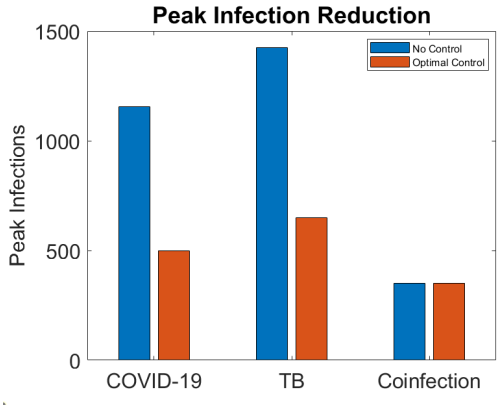

(C) Peak infection reduction

FIGURE 3. Impact of intervention strategies on disease transmission.

Figure 4 presents a comparison of infection levels with and without the implementation of control measures. In Figure 4a, the COVID–19 infection levels are significantly higher when no control strategies are applied. Similarly, Figure 4b demonstrates that when the best control measures are used, the overall infection levels are significantly lowered.

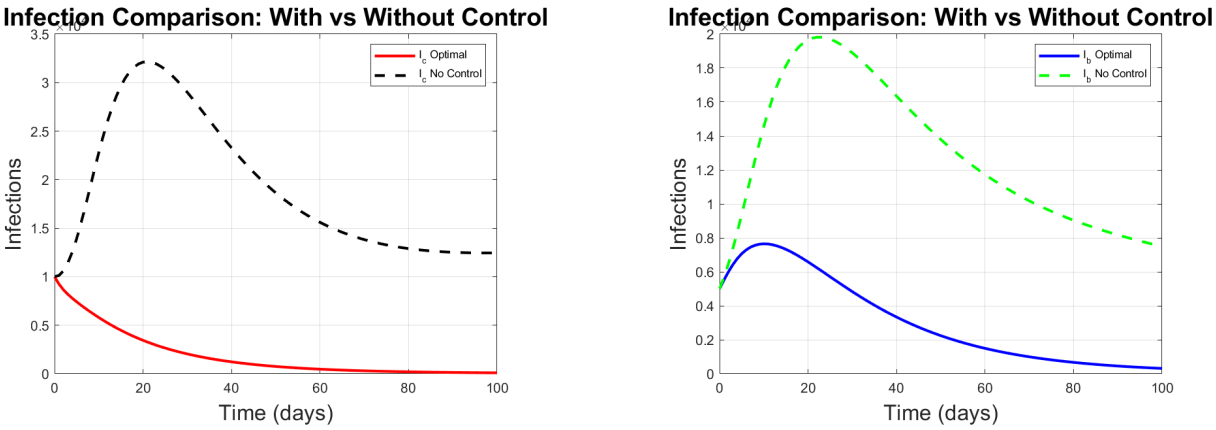

(A) COVID-19 infection comparison (B) Infections with and without control

FIGURE 4. Comparison of infection levels with and without control measures.

The economic implications of the control strategies are illustrated in Figure 5. Figure 5a demonstrates the cost function's convergence throughout the optimization phase, showing that the numerical technique was effective in finding the best control solution.Figure 5b presents the distribution of costs among the different control strategies, highlighting how resources are allocated among distancing, vaccination, and treatment. Vaccination takes the largest amount followed by treatment as represented in the pie chart.

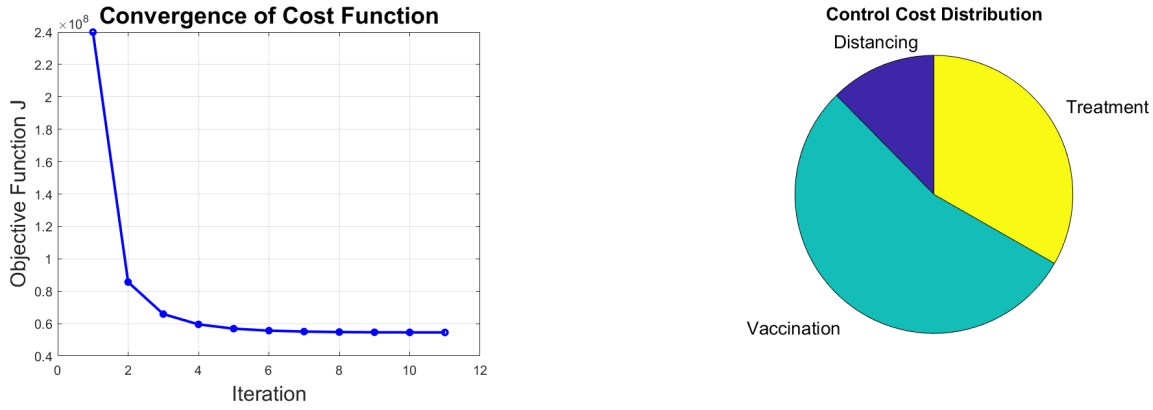

(A) Convergence of cost function (B) Control cost distribution

FIGURE 5. Cost analysis of optimal control strategies.

Lastly, Figure 6 depicts the population's final distribution among the epidemiological compartments at the conclusion of the simulation period showing the long-term result of the epidemic. The findings show that only a small portion of the population is still infected, with the majority remaining in the susceptible or recovered classifications. This result shows that the population's overall disease burden is much decreased when the best management measures are put in place.

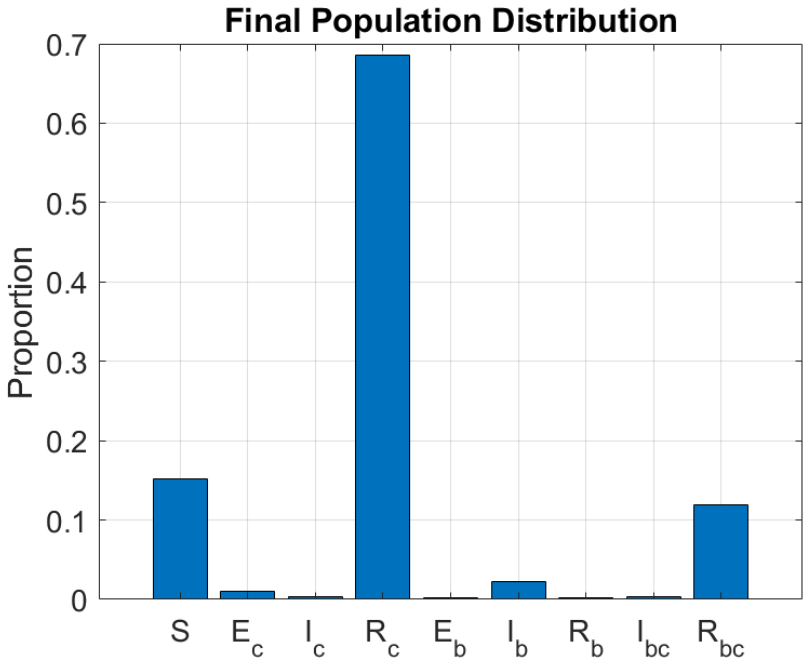

FIGURE 6. Final population distribution among the epidemiological compartments.

4. DISCUSSION AND CONCLUSIONS

4.1. Discussion. In order to examine the transmission dynamics of TB and COVID-19 co-infection, this study formulated a deterministic compartmental model that included time delays and the most effective control techniques. The inclusion of diagnostic and treatment delays in our model provides a timely recognition of the disease thus predicting the disease progression compared to classical models without delays.The analytical results show that the disease-free equilibrium is locally asymptotically stable when the basic reproduction number is less than unity. However, the presence of backward bifurcation indicates that reducing R_0 below one

is not sufficient to eliminate the disease. This implies that even when transmission appears to be under control, the disease may persist in the population due to co-infection dynamics and delayed interventions.

The numerical simulations indicates that COVID-19 infections increase rapidly due to shorter incubation periods, whereas TB infections persist longer due to their chronic nature. Co-infection cases remain relatively lower but play a critical role in sustaining transmission. The results further demonstrates that combined intervention strategies are significantly more effective than single control measures. Social distancing reduces early transmission, vaccination provides long-term protection, and treatment reduces infectiousness and disease-induced mortality. However, the success of these control efforts is greatly reduced by delays in diagnosis and treatment.

The findings obtained are consistent with existing literature on infectious disease co-infection models, where delays and interaction between diseases increase the overall disease burden. The study also explains the importance of integrating TB and COVID-19 control strategies, particularly in resource-limited settings where healthcare access is limited.

4.2. Conclusion. In this work, we conducted a thorough analysis of the deterministic epidemiological mathematical model for the dynamics of COVID-19 co-infection and tuberculosis (TB) transmission in a community. The aim of this study was to fully understand how the two illnesses interact and assess how various control strategies can reduce the spread of the infection within a community. To get a clear understanding of the public health burden related to COVID-19 and tuberculosis, the study included some epidemiological aspects such as exposure, infections, recovery, declining immunity, treatment, and co-infection dynamics.

The formulated model divided the population into nine different epidemiological compartments representing susceptible individuals, exposed individuals, infectious individuals, recovered individuals and co-infected individuals. This made it possible to study how individuals move from one disease state to another within a given time. By including both single infections and co-infections, the model was able to capture the complex interaction between TB and COVID-19 which remains to be a great concern in many countries, especially in developing countries where TB prevalence is still high.

The study shows that the transmission dynamics of TB and COVID-19 is triggered by the forces of infection associated with each disease. The results showed that increased contact between susceptible individuals and infectious individuals contributes significantly to the rise in disease prevalence. This means that the co-infected individuals increase the overall disease burden because co-infection weakens the immune system and increase the likelihood of serious health complications. The model therefore proved that TB and COVID-19 can reinforce one another within a population making disease control more difficult when the two diseases exist simultaneously.

The qualitative analysis of the model provided important insights of the disease system. Positivity of solutions was established showing that all state variables remain non-negative all through which confirms that the model is epidemiologically meaningful. Boundedness of the solutions was also proved showing that the total population remains bounded within the feasible region. These properties proved the mathematical validity of the model solutions and ensured that the model results are biologically feasible.

The disease-free equilibrium point of the model was determined in order to understand conditions in which the disease can be eliminated from the population. The basic reproduction number was calculated using the next generation matrix method. The analysis showed that when $R_0 < 1$ the disease dies out from the population. However, when $R_0 > 1$ the diseases persist and continues spreading within the community.

Numerical simulations was also done to support the analytical findings and to provide a clear understanding of the disease behavior over time. The simulation results showed that susceptible individuals decreases when transmission rates are high, while exposed and infectious populations increases at the time. In the absence of intervention measures, the number of infected and co-infected individuals remains high for a long period of time. However, when effective control measures are introduced, the simulations shows a decrease in the number of the infections.

The study also investigated the impact of different control strategies on disease transmission. The results indicated that combined intervention strategies are more effective than when using a single intervention approach. Vaccination reduced the number of susceptible individuals at risk

of contracting COVID-19 infection, while treatment reduced TB transmission and its progressions. Public health measures such as social distancing, use of face masks, creating awareness campaigns and early diagnosis also contributed greatly to reducing the spread of infection.

The findings from previous studies shows that TB and COVID-19 remains a global public health threats, especially when they occur simultaneously. Researchers have found out that individuals with TB who acquire COVID-19 experiences more severe clinical outcomes, including increased morbidity and mortality, due to compromised respiratory function and weakened immunity [24, 25]. Research also suggests that COVID-19 may accelerate the progression of latent TB to active TB thereby increasing the burden of co-infection [24]. Additionally, the COVID-19 pandemic also disrupted TB diagnosis, treatment and control programs worldwide leading to a delayed detection, treatment and a great rise in TB-related deaths after years of decline [3, 26]. These findings indicates that there is urgent need for integrated intervention strategies that are capable of addressing the dual burden of TB and COVID-19. For that reason, this study seek to curb this gap through formulating a delayed mathematical model incorporating the optimal control.

The results of this study have significant impact for illness management and public health policy. Public awareness campaigns, accessible healthcare services, and integrated disease monitoring should all receive more funding from the government and health organizations. The introduction of COVID-19 poses additional difficulties in areas with high TB prevalence, demanding combined intervention methods. The burden of co-infection might be eased by supporting the healthcare systems and guaranteeing a sufficient supply of medicine.

This study contributes to the growing sector of infectious disease modeling by providing a mathematical framework for understanding TB and COVID-19 co-infection dynamics. The model can be useful to researchers, policymakers, and public health practitioners in designing and evaluating disease intervention strategies. Also, the study demonstrates how mathematical modeling can be applied as an important tool in predicting disease behavior and guiding evidence-based decision making.

Despite the important findings obtained in this study, we also noted some limitations in that, the model considered a homogeneous population meaning that all individuals have equal

chances of interaction. Commonly, contact patterns vary according to age, occupation, location, and social behavior. Another limitation is that the study used some parameter values obtained from the review of the literature and assumptions due to limited availability of the epidemiological data on these two diseases.

The model, however, emphasizes the importance of integrated disease control approaches and provides significant information on the dynamics of TB and COVID-19 co-infection. Future research may include population variability, such as age distribution or differences in immunity levels. These factors can influence disease transmission and provide a more realistic picture of the disease dynamics. This would assist policymakers in determining the most effective method for preventing the spread of the two diseases. In conclusion, excellent treatment programs, immunization campaigns, public awareness campaigns, and strong public health policies are all required to control COVID-19 and tuberculosis simultaneously.

CONFLICT OF INTERESTS

The authors declare that there is no conflict of interests.

REFERENCES

[1] World Health Organization, Global Tuberculosis Report 2020, 2020. https://www.who.int/publications/i/item/9789240013131.

[2] A.B. Hogan, B.L. Jewell, E. Sherrard-Smith, J.F. Vesga, O.J. Watson, et al., Potential Impact of the COVID-19 Pandemic on HIV, Tuberculosis, and Malaria in Low-Income and Middle-Income Countries: a Modelling Study, Lancet Glob. Health 8 (2020), e1132–e1141. https://doi.org/10.1016/s2214-109x(20)30288-6.

[3] World Health Organization, Global Tuberculosis Report 2021, 2021. https://www.who.int/publications/i/item/9789240037021.

[4] C. McQuaid, N. McCreesh, J.M. Read, T. Sumner, C. COVID-19 Working Group, et al., The Potential Impact of COVID-19-Related Disruption on Tuberculosis Burden, Eur. Respir. J. 56 (2020), 2001718. https://doi.org/10.1183/13993003.01718-2020.

[5] M. Tadolini, L.R. Codecasa, J.M. García-García, F.X. Blanc, S. Borisov, et al., Active Tuberculosis, Sequelae and COVID-19 Co-infection: First Cohort of 49 Cases, Eur. Respir. J. 56 (2020), 2001398. https://doi.org/10.1183/13993003.01398-2020.

[6] M.J. Saunders, C.A. Evans, COVID-19, Tuberculosis and Poverty: Preventing a Perfect Storm, Eur. Respir. J. 56 (2020), 2001348. https://doi.org/10.1183/13993003.01348-2020.

[7] M. Pai, M.A. Behr, D. Dowdy, K. Dheda, M. Divangahi, et al., Tuberculosis, Nat. Rev. Dis. Prim. 2 (2016), 16076. https://doi.org/10.1038/nrdp.2016.76.

[8] I. Motta, R. Centis, L. D'Ambrosio, J. García-García, D. Goletti, et al., Tuberculosis, COVID-19 and Migrants: Preliminary Analysis of Deaths Occurring in 69 Patients from Two Cohorts, Pulmonology 26 (2020), 233–240. https://doi.org/10.1016/j.pulmoe.2020.05.002.

[9] R. Crisan-Dabija, C. Grigorescu, C.A. Pavel, B. Artene, I.V. Popa, et al., Tuberculosis and COVID-19: Lessons from the Past Viral Outbreaks and Possible Future Outcomes, Can. Respir. J. 2020 (2020), 1401053. https://doi.org/10.1155/2020/1401053.

[10] S. Ruan, Delay Differential Equations in Single Species Dynamics, in: O. Arino, M. Hbid, E.A. Dads, (eds) Delay Differential Equations and Applications, NATO Science Series, Vol 205, Springer, Dordrecht, (2006). https://doi.org/10.1007/1-4020-3647-7_11.

[11] E. Beretta, Y. Kuang, Modeling and Analysis of a Marine Bacteriophage Infection with Latency Period, Nonlinear Anal. Real World Appl. 2 (2001), 35–74. https://doi.org/10.1016/s0362-546x(99)00285-0.

[12] F. Brauer, C. Castillo-Chavez, Mathematical Models in Population Biology and Epidemiology, Springer, 2012. https://doi.org/10.1007/978-1-4614-1686-9.

[13] H.W. Hethcote, The Mathematics of Infectious Diseases, SIAM Rev. 42 (2000), 599–653. https://doi.org/10.1137/s0036144500371907.

[14] Z. Liu, P. Magal, O. Seydi, G. Webb, A COVID-19 Epidemic Model with Latency Period, Infect. Dis. Model. 5 (2020), 323–337. https://doi.org/10.1016/j.idm.2020.03.003.

[15] D. Okuonghae, A. Omame, Analysis of a Mathematical Model for COVID-19 Population Dynamics in Lagos, Nigeria, Chaos Solitons Fractals 139 (2020), 110032. https://doi.org/10.1016/j.chaos.2020.110032.

[16] J.S. Lopes, P. Rodrigues, S.T. Pinho, R.F. Andrade, R. Duarte, et al., Interpreting Measures of Tuberculosis Transmission: A Case Study on the Portuguese Population, BMC Infect. Dis. 14 (2014), 340. https://doi.org/10.1186/1471-2334-14-340.

[17] F. Inayaturohmat, N. Anggriani, A.K. Supriatna, A Mathematical Model of Tuberculosis and COVID-19 Coinfection with the Effect of Isolation and Treatment, Front. Appl. Math. Stat. 8 (2022), 958081. https://doi.org/10.3389/fams.2022.958081.

[18] A. Omame, M. Abbas, C.P. Onyenegecha, A Fractional-Order Model for COVID-19 and Tuberculosis Co-infection Using Atangana–Baleanu Derivative, Chaos Solitons Fractals 153 (2021), 111486. https://doi.org/10.1016/j.chaos.2021.111486.

[19] S. Bandekar, M. Ghosh, A Co-Infection Model on TB - COVID-19 with Optimal Control and Sensitivity Analysis, Math. Comput. Simul. 200 (2022), 1–31. https://doi.org/10.1016/j.matcom.2022.04.001.

[20] S. Paul, A. Mahata, U. Ghosh, B. Roy, Study of SEIR Epidemic Model and Scenario Analysis of COVID-19 Pandemic, Ecol. Genet. Genomics 19 (2021), 100087. https://doi.org/10.1016/j.egg.2021.100087.

[21] K.G. Mekonen, S.F. Balcha, L.L. Obsu, A. Hassen, Mathematical Modeling and Analysis of TB and COVID-19 Coinfection, J. Appl. Math. 2022 (2022), 2449710. https://doi.org/10.1155/2022/2449710.

[22] M.S. Goudiaby, L.D. Gning, M.L. Diagne, B.M. Dia, H. Rwezaura, et al., Optimal Control Analysis of a COVID-19 and Tuberculosis Co-dynamics Model, Inform. Med. Unlocked 28 (2022), 100849. https://doi.org/10.1016/j.imu.2022.100849.

[23] S. Edward, A Deterministic Mathematical Model for Direct and Indirect Transmission Dynamics of Typhoid Fever, OALib 04 (2017), e3493. https://doi.org/10.4236/oalib.1103493.

[24] A. Mishra, A.A. George, K.K. Sahu, A. Lal, G. Abraham, Tuberculosis and COVID-19 Co-infection: An Updated Review, Acta Biomed. Atenei Parm. 92 (2020), e2021025. https://doi.org/10.23750/abm.v92i1.10738.

[25] Q. Wang, Y. Cao, X. Liu, Y. Fu, J. Zhang, et al., Systematic Review and Meta-Analysis of Tuberculosis and COVID-19 Co-infection: Prevalence, Fatality, and Treatment Considerations, PLOS Negl. Trop. Dis. 18 (2024), e0012136. https://doi.org/10.1371/journal.pntd.0012136.

[26] World Health Organization, Global Tuberculosis Report 2024, 2024. https://www.who.int/teams/global-programme-on-tuberculosis-and-lung-health/tb-reports/global-tuberculosis-report-2024.